SCIENTIFIC REPORTS

OPEN

Plasmon-Enhanced Photoelectrochemical Current and Hydrogen Production of (MoS_2-TiO_2)/Au Hybrids

Received: 17 May 2017
Accepted: 27 June 2017
Published online: 3 August 2017

Ying-Ying Li[1], Jia-Hong Wang[1,2], Zhi-Jun Luo[1], Kai Chen[1,3], Zi-Qiang Cheng[1], Liang Ma[1], Si-Jing Ding[1], Li Zhou[1] & Qu-Quan Wang[1,3]

Three component hybrid (MoS_2-TiO_2)/Au substrate is fabricated by loading plasmonic Au nanorods on the MoS_2 nanosheets coated TiO_2 nanorod arrays. It is used for photoelectrochemical (PEC) cell and photocatalyst for hydrogen generation. Owing to the charge transfer between the MoS_2-TiO_2 hetero-structure, the PEC current density and hydrogen generation of TiO_2 nanoarrays are enhanced 2.8 and 2.6 times. The broadband photochemical properties are further enhanced after Au nanorods loading. The plasmon resonance of Au nanorods provides more effective light-harvesting, induces hot-electron injection, and accelerates photo-excited charges separation. The results have suggested a route to construct nanohybrid by combining one-dimensional arrays and two-dimensional nanosheets, meanwhile have successfully utilized plasmonic nanorods as a sensitizer to improve the photochemical properties of the semiconductor nanocomposite.

As a member of layered two-dimensional material, molybdenum disulfide (MoS_2) is promising for the applications in energy and environment[1–10]. The MoS_2 nanosheets could be achieved by break the interlayer van der Waals forces. The band gap of MoS_2 nanosheets is seriously depended on its layer number, which is varied from 1.3 (bulk) to 1.8 eV (monolayer)[11–14]. Therefore, the few-layered MoS_2 could be used as an efficient visible light harvester. Meanwhile, the two-dimensional structure provides large contact interface and efficient charge transfer, as a result, the layered MoS_2 nanosheets have been regarded as a low-cost co-catalyst candidate resently[15–22]. TiO_2 is a wide band gap (3.6 eV) semiconductor and has exhibited potential in photoelectrochemical (PEC) water splitting and photocatalytic applications[23–29]. The narrow band gap of MoS_2 can broaden the visible-light response. Additionally, the interface charge transfer between MoS_2-TiO_2 hetero-junction would accelerate the charge separation and enhance photocatalytic activity and increase the hydrogen generation[28–36].

Gold nanoparticles (NPs) supporting tunable surface plasmon resonance in a wide region have been used for various light-matter interaction enhancement[37–41], in which the main mechanism are broadening light-harvesting region and facilitating the charge separation[42–47]. Yung-Jung Hsu *et al.* have reported that the hot electrons in Au NPs can get over the Schottky barrier and be injected into the conduction band of the TiO_2, which would supply additional charge carriers for photocatalytic reaction[48]. Xing-Hua Xia *et al.* also reported an efficient water splitting hydrogen evolution reaction of Au nanorods/MoS_2 nanosheets hybrids through increase the carrier density in MoS_2 by Au nanorods[49].

In this paper, we report a three component hybrid (MoS_2-TiO_2)/Au including two-dimensional MoS_2 nanosheets, self-ordered TiO_2 nanorod arrays, and plasmonic Au nanorods. The microscopic structures and optical properties of (MoS_2-TiO_2)/Au are characterized. The photochemical activities of TiO_2, MoS_2-TiO_2, and (MoS_2-TiO_2)/Au are comparatively investigated. The physical mechanisms of enhanced light-harvesting, hot electrons injection, and acceleration of separation of photo-excited charges are further discussed.

[1]Key Laboratory of Artificial Micro- and Nano-structures of the Ministry of Education, and School of Physics and Technology, Wuhan University, Wuhan, 430072, P. R. China. [2]Institute of Biomedicine and Biotechnology, Shenzhen Institutes of Advanced Technology, Chinese Academy of Sciences, Shenzhen, 518055, P. R. China. [3]The Institute for Advanced Studies, Wuhan University, Wuhan, 430072, P. R. China. Ying-Ying Li, Jia-Hong Wang and Zhi-Jun Luo contributed equally to this work. Correspondence and requests for materials should be addressed to S.-J.D. (email: sjding@whu.edu.cn) or L.Z. (email: zhouli@whu.edu.cn) or Q.-Q.W. (email: qqwang@whu.edu.cn)

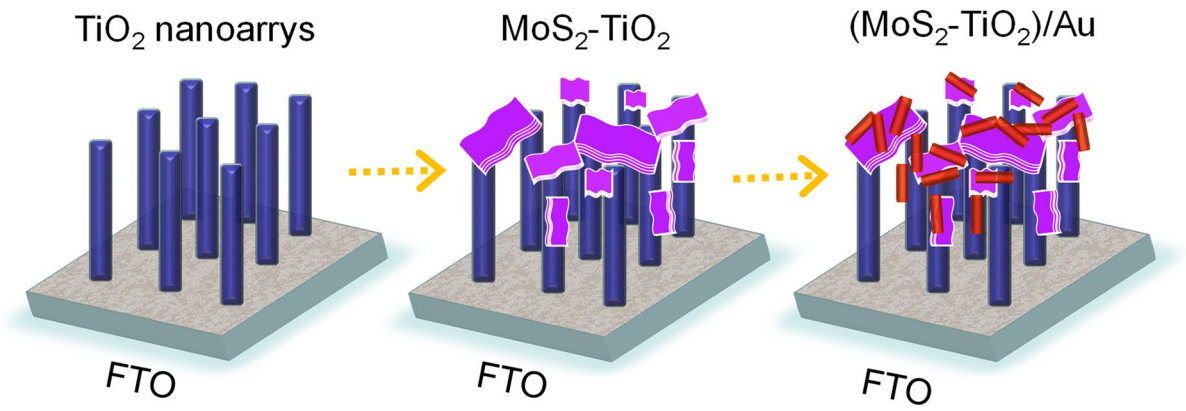

Figure 1. Schematic illustration of preparing (MoS_2-TiO_2)/Au nanocomposites.

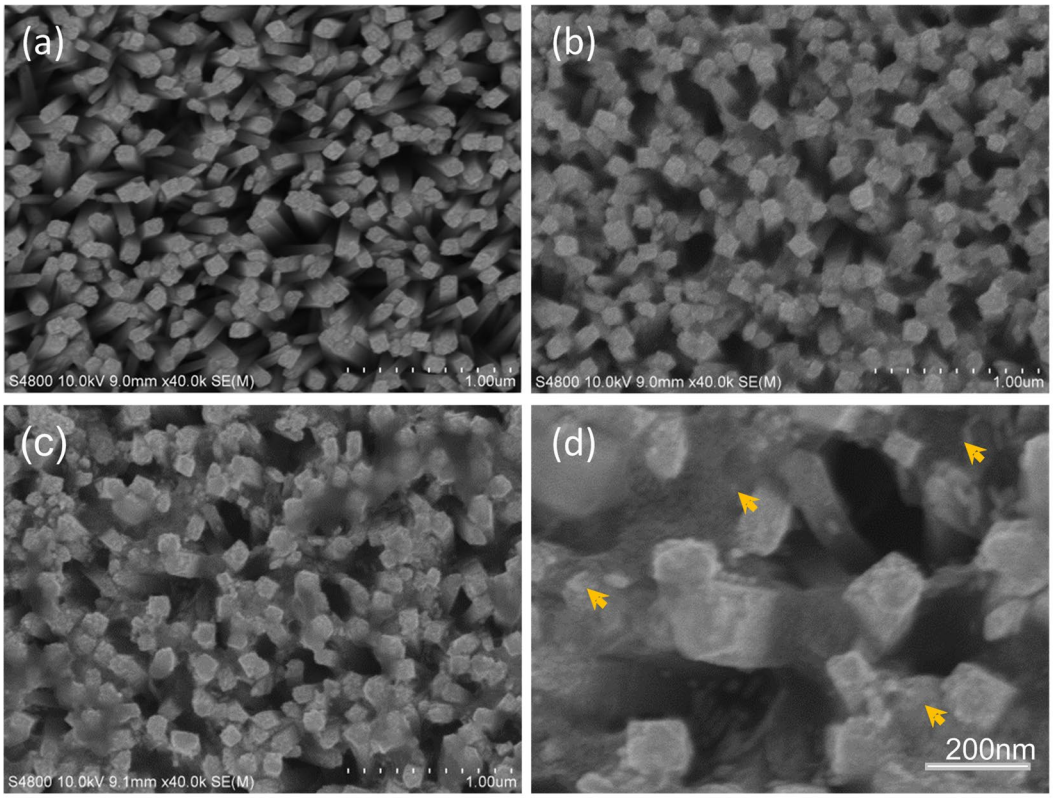

Figure 2. Microscopic structure evolution in prepration of (MoS_2-TiO_2)/Au. (**a**–**d**) Top-view SEM images of TiO_2 (**a**), MoS_2-TiO_2 (**b**), and (MoS_2-TiO_2)/Au (**c**,**d**). The arrows in (**d**) indictae the locations of Au nanorods.

Results and Discussion

The preparation procedure of (MoS_2-TiO_2)/Au is shown in Fig. 1. The TiO_2 nanorod arrays are firstly grown on the conductive FTO glass substrate. Then layered MoS_2 nanosheets are deposited onto the TiO_2. Finally, the as-prepared Au nanorods are introduced by a drop-casting method. As shown in Fig. 2a, the TiO_2 nanorods are vertically grown from the FTO conductive glass. The average lateral dimension of TiO_2 NRs is about 80 nm. Figure 2b shows the sheet-shaped MoS_2 cover up the top of TiO_2 nanorods and are also grown into the interspace of nanorod array. The estimated side-length of MoS_2 nanosheets is in the range from hundreds of nanometers to micrometer-scale. The dimension and amount of MoS_2 nanosheets can be controlled by the deposition reaction time. As the magnification TEM image shown in Fig. 2d, the locations of Au nanorods are randomly distributed on the MoS_2-TiO_2, including on the basal plane of MoS_2 nanosheets, on the top-end and side-surface of TiO_2 nanorods, and even on the junction of MoS_2-TiO_2.

For verifying the component in the hybrids, the HRTEM images and EDX analysis of the (MoS_2-TiO_2)/Au composites are shown in Fig. 3. The samples are extracted from the FTO glass and placed on the copper grids for

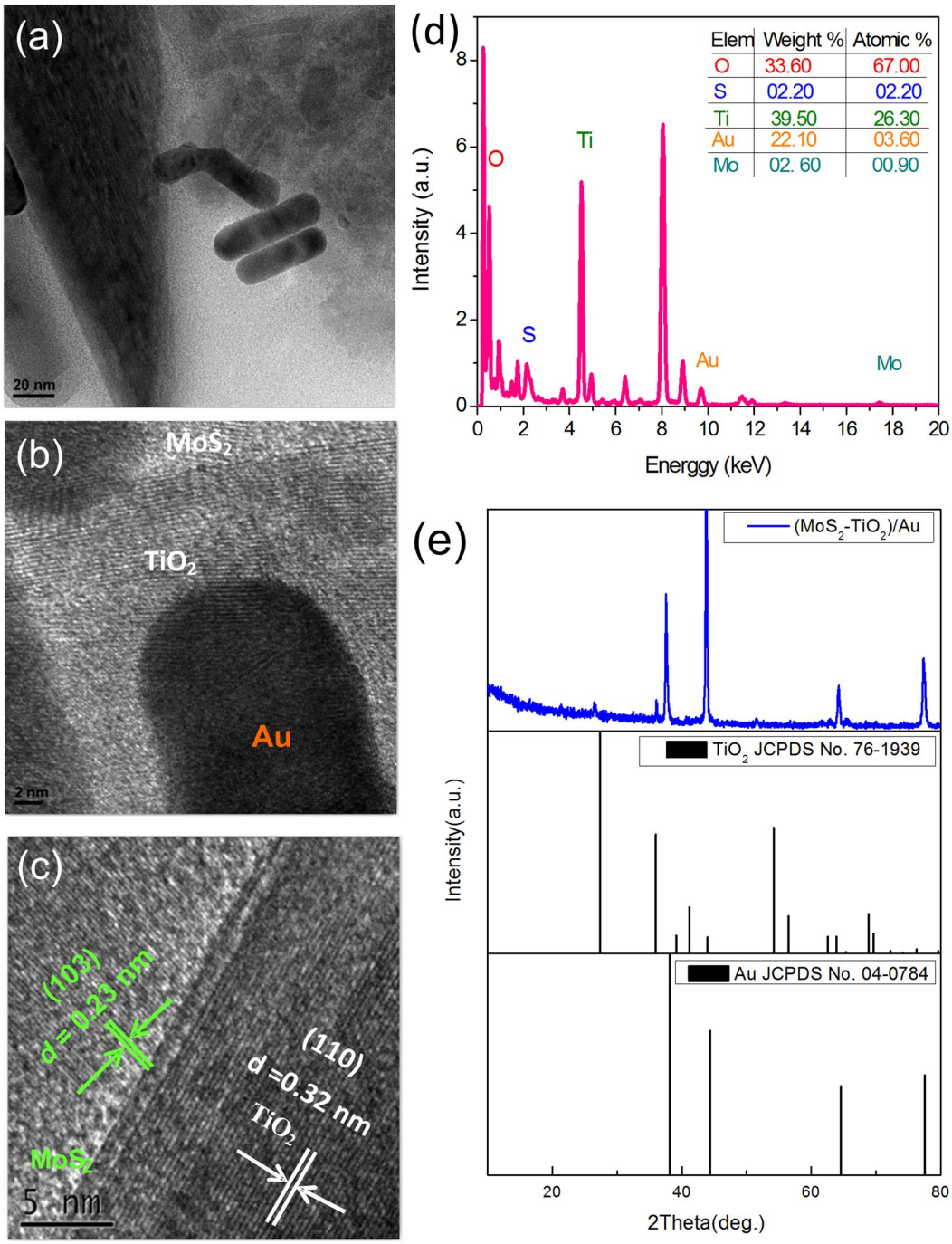

Figure 3. Component analysis of the (MoS_2-TiO_2)/Au composites. (**a**–**c**) HRTEM images (**d**) EDX and (**e**) XRD pattern of (MoS_2-TiO_2)/Au composites.

TEM observation. The observed Au nanorods have the transverse size of 15 nm and the aspect ratio in the range of 3–4. The lattice fringes of an individual TiO_2 nanorod with a spacing of 0.32 nm can be assigned to the (110) lattice planes of rutile TiO_2. The MoS_2 nanosheets show the lattice fringes with 0.23 nm spacing, corresponding to the (103) planes of MoS_2. The EDX analysis of the prepared (MoS_2-TiO_2)/Au is presented in Fig. 3d. The composite mainly contains Ti and O, and the rest of the trace elements are S, Au, and Mo. The atomic ratios of Mo: S and Ti: O are both approximately 1: 2. In the XRD pattern (Fig. 3e), two sets of diffraction peaks are present, which are assigned to the TiO_2 nanorod array phase (JCPDS No. 76-1939) and Au nanorods phase (JCPDS No. 04-0784).

Figure 4 displays the absorption spectra of pure TiO_2, MoS_2-TiO_2, and (MoS_2-TiO_2)/Au. Pure TiO_2 only absorbs UV light and exhibits an intense absorption edge before 400 nm, attributing to its band gap of 3.2 eV. The few-layered MoS_2 nanosheets are reported to have two absorption bands near 400 nm and 600 nm in the visible region[36], which are shown in the spectrum of MoS_2-TiO_2. In the experiment, the sample was tuned to

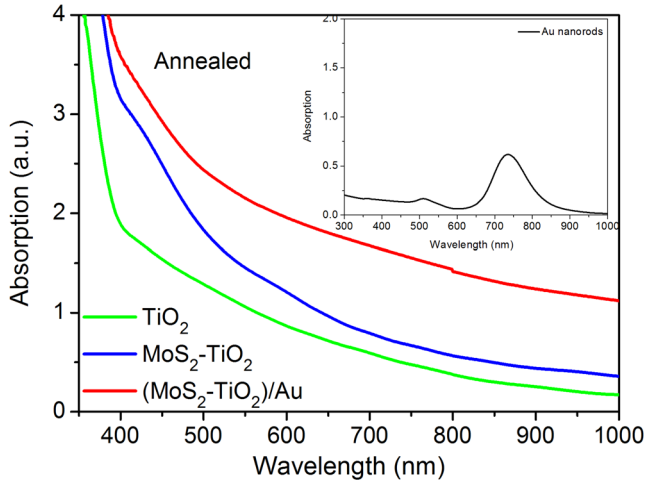

Figure 4. Absorption spectra of pure TiO_2, MoS_2-TiO_2, and (MoS_2-TiO_2)/Au. The inset shows the absorption spectrum of as-prepared AuNRs.

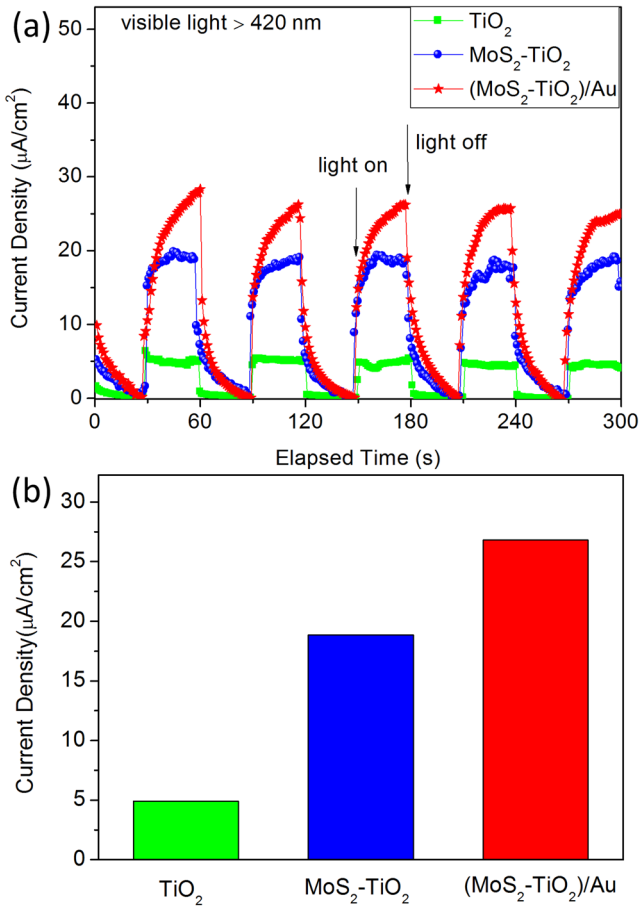

Figure 5. Photocurrent responses of TiO_2, MoS_2-TiO_2, (MoS_2-TiO_2)/Au electrodes recorded in 0.1 M Na_2SO_3 and Na_2S aqueous solution under visible light by light-on and light-off cycles.

yellowish-brown color when the MoS_2 nanosheets were grown onto the TiO_2. These results indicate the deposited MoS_2 nanosheets have efficient light-harvesting in visible region. The absorption intensity around 700 nm of (MoS_2-TiO_2)/Au is obviously enhanced, which is attributed to the plasmon of Au nanorods.

The photon-electron conversion performance was performed by measuring the photocurrent response of three-electrode PEC cells with the hybrids as photoanode. Figure 5a shows the PEC $I-t$ curves of the TiO_2, MoS_2-TiO_2, and (MoS_2-TiO_2)/Au under the visible-light irradiation (wavelength >420 nm) with a bias of

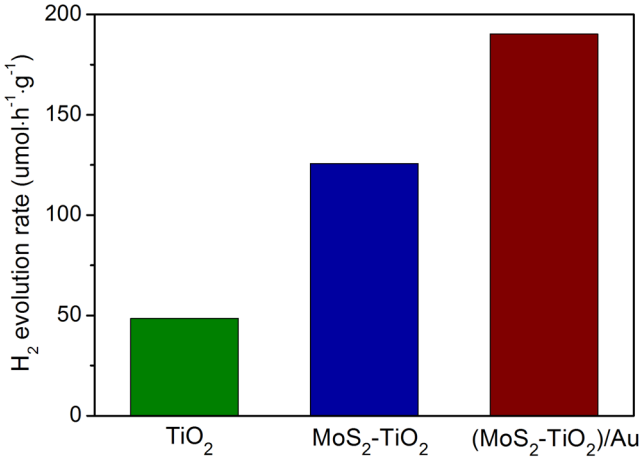

Figure 6. Photocatalytic hydrogen production activities of TiO_2, MoS_2-TiO_2, (MoS_2-TiO_2)/Au electrodes under full spectrum in the aqueous solution containing 20% methanol as sacrificial agents.

0.6 V versus Ag/AgCl reference electrode. The electrolyte including Na_2SO_3 and Na_2S solution can consume photo-excited holes on the photoanode. The photo-excited electrons are migrated to the Pt counter electrode through external bias circuit. As the arrows indicated in Fig. 5a, the light irradiation is switched ON/OFF for assessing the photocurrent responses. The average photocurrent densities of the three samples are plotted as bar charts in Fig. 5b. The current densities are 4.9, 18.9, 26.8 $\mu A/cm^2$, for the samples of TiO_2, MoS_2-TiO_2, (MoS_2-TiO_2)/Au, respectively. The current density of (MoS_2-TiO_2)/Au is 5.5 times that of TiO_2 and 1.42 times that of MoS_2-TiO_2.

The pure TiO_2 electrode shows a considerably low photocurrent density, because TiO_2 has large band bap and only responds to UV light. The enhanced photocurrent response of MoS_2-TiO_2 electrode can be understood through two aspects of enhanced visible light absorption and accelerated photo-excited charge separation. As discussed in Fig. 4, MoS_2 nanosheets exhibit efficient light absorption in visible region. The jungle-typed microstructure of TiO_2 nanorod arrays could trap the incident light inside the arrays through multiple scatterings/reflections and guide the light pass through the MoS_2 nanosheets multiply times, enhancing the visible light-harvesting. In addition, the band alignment between MoS_2 and TiO_2 is favorable for the electron transfer from the conduction band (CB) of MoS_2 to the CB of TiO_2 and suppresses the photogenerated carrier recombination of TiO_2 effectively. Moreover, the inserted MoS_2 nanosheets connect neighboring TiO_2 nanorods and act as bridge routes which benefit the electron transfer along the TiO_2 channel to the conductive substrate.

The highest photocurrent of (MoS_2-TiO_2)/Au electrode is benefits from the plasmon-enhanced light absorption and the plasmon-induced hot electron injections. In detail, the Au nanorods work as a reaction sensitizer and enhance the visible light absorption ability of MoS_2. On the other hand, the Au nanorods have intense plasmon absorption and the plasmon-produced energetic electrons in the (MoS_2-TiO_2)/Au nanosystem could also contribute to the photon-to-electron conversion. The hot electrons can get over the Schottky barrier and be injected into the CB of MoS_2 and TiO_2.

Finally, the hot electron injection of Au nanorods, the enhanced visible light-harvesting and the accelerated charge separation in the (MoS_2-TiO_2)/Au hybrids is further demonstrated by testing the photocatalytic hydrogen generation. The H_2 evolution rate of TiO_2 and MoS_2-TiO_2 under visible light are barely observed, while that of (MoS_2-TiO_2)/Au is enhanced. Figure 6 shows the photocatalytic hydrogen generation under full spectrum, TiO_2 alone shows a low photocatalytic activity with the H_2 evolution rate of 48 $\mu mol \cdot h^{-1} \cdot g^{-1}$ because of the rapid recombination of electron-hole pairs. The introduction of MoS_2 results in a significant improvement of photocatalytic H_2 evolution rate to 125 $\mu mol \cdot h^{-1} \cdot g^{-1}$. The MoS_2-TiO_2 composite photocatalysts show enhanced photocatalytic activity because the layered MoS_2 can help the charge separation also act as an efficient co-catalyst for H_2 generation than TiO_2. In the presence of a small amount of Au nanorods in the hybrid photocatalysts, the photocatalytic H_2 evolution rate of (MoS_2-TiO_2)/Au hybrids is further enhanced to 190 $\mu mol \cdot h^{-1} \cdot g^{-1}$. The experimental result of photocatalytic hydrogen generation is consistent with that of the photocurrents under visible light. Figure S1 shows the photocatalytic hydrogen generation under visible light. The corresponding energy band structure and electrons transfer mechanism is schematically shown in the Fig. 7.

Conclusion

In conclusion, we have prepared a composite of (MoS_2-TiO_2)/Au consisting of two-dimensional MoS_2 nanosheets, self-ordered TiO_2 nanorod arrays, and plasmonic Au nanorods. Acting as photoanode of PEC cells and photocatalysts for hydrogen generation, the current density of TiO_2 is increased 2.8 times and the hydrogen generation rate is increased 2.6 time via the charge transfer from MoS_2 nanosheets. Moreover, the PEC current density and hydrogen generation rate of MoS_2-TiO_2 is further enhanced 42% and 52% by plasmon resonance of Au nanorods. The intimate and large contact interface between AuNRs and MoS_2-TiO_2 leads to the efficient injection of hot electron, which plays a key factor in determining the high photocurrent response of (MoS_2-TiO_2)/Au. The efficient visible light absorption and the high carrier mobility of layered MoS_2 nanosheets contribute

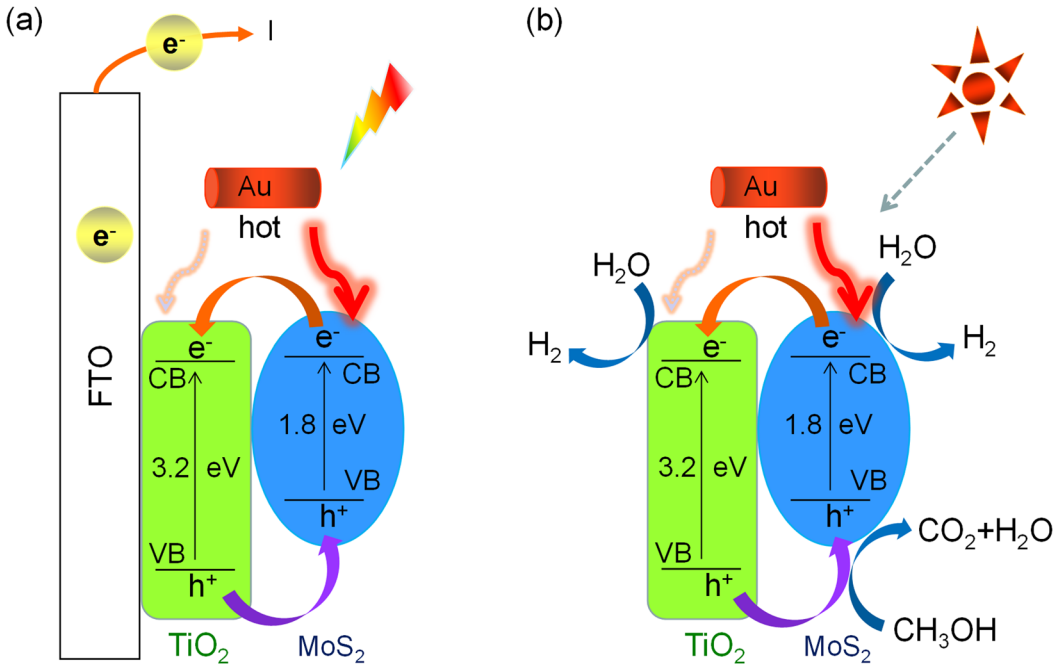

Figure 7. Schematic illustration of energy band structure and electron-hole separation of (MoS_2-TiO_2)/Au nanocomposites in PEC cell (**a**) and in photocatalytic hydrogen generation (**b**).

the photocurrent response. In addition, the array-typed nanostructure can effectively trap incident light and the MoS_2-TiO_2 hetero-junction can lead to efficient photo-excited charge separation.

Methods

Materials Synthesis. Titanium butoxide (TBT, ≥99%), hydrochloric Acid (HCl, 37%), sodium molybdate ($Na_2MoO_4 \cdot 2H_2O$, ≥99%), thioacetamide (TAA, ≥99%). All chemical materials were used without further purification.

Synthesis of TiO_2 Nanorod Arrays on FTO. TiO_2 nanorod arrays were fabricated on the FTO substrate through a hydrothermal method[50]. Before modification, the FTO substrates were washed with acetone, ethanol in an ultrasonic washer for 5 minutes. Then, 0.4 g of titanium butoxide was dissolved into 30 mL of 6 M HCl aqueous solution and then transferred into a Teflon-lined steel autoclave with a capacity of 50 mL. The FTO substrates were placed against the Teflon wall with the FTO side facing down. The autoclave was heated in an oven at 150 °C for 6 h and then cooled down to room temperature. The TiO_2 nanorods were cleaned with deionized water and ethanol.

Synthesis of MoS_2 on TiO_2. 0.3 g of sodium molybdate ($Na_2MoO_4 \cdot 2H_2O$) and 0.6 g of **thioacetamide** were added. After stirring for 5 minutes, the reaction solution was transferred into a 50 mL Teflon-lined stainless steel autoclave and kept in an electric oven at 200 °C for 10 h. The autoclave was then cooled down to room temperature in the oven.

Synthesis of (MoS_2-TiO_2)/Au. Au nanorods of various aspect ratios were synthesized using a seed-mediated growth method in aqueous solution[51]. Then, the as-prepared Au nanorods were dropped onto the FTO grown with the MoS_2-TiO_2 nanocomposites. The samples were thermally treated at 350 °C in N_2 atmosphere for 0.5 h, and then dried at 70 °C for 10 h.

Characterizations. Transmission electron microscopy (TEM) and high-resolution TEM (HRTEM) images were taken on a JEOL 2100 F transmission electron microscope at an accelerating voltage of 200 kV. Energy-dispersive X-ray spectra (EDX) analysis was performed on an energy-dispersive X-ray spectrometer incorporated in the HRTEM. Scanning electron microscope (SEM) measurements were carried out with an FEI Sirion 200 scanning electron microscope operated at an accelerating voltage of 10.0 kV. Extinction spectra were recorded by the ultraviolet-visible-near infrared (UV-Vis-NIR) spectrophotometers (TU-1810 and Varian Cary 5000).

Photoelectrochemical Activity Measurement. A three-electrode configuration was adopted in a quartz cell on the VersaSTAT 3 electrochemical workstation (AMETEK, Inc., United States). A Pt plate and a commercially available Ag/AgCl electrode are used as the counter and reference electrodes respectively, and the sample modified FTO electrode was used as the work electrode. The 0.1 M Na_2SO_3 and Na_2S aqueous solution was prepared to support electrolyte. The effective surface area of the work electrode was $1 \times 2.5\ cm^2$. Before measurement,

the as-prepared samples of TiO_2, MoS_2-TiO_2, (MoS_2-TiO_2)/Au were thermally treated at 350 °C in high-purity nitrogen atmosphere for 0.5 h. A 300 W Xenon lamp equipped with an ultraviolet cut-off filter ($\lambda > 420$ nm) was used as light source.

Photocatalytic H_2 Evolution. Before measurement, the samples were dried at 70 °C for 10 h. The photocatalytic hydrogen evolution tests were conducted in a quartz reactor tube with a rubber septum. 20 mg photocatalyst powders were dispersed in 50 mL of aqueous solution containing 20% of methanol as sacrificial reagents. The system was evacuated by using a pump and the reaction solution was stirred for 30 min to remove any dissolved air. The light source was a 300 W Xenon lamp. The temperature of the suspension was maintained by an external water cooling system. The amount of hydrogen gas was automatically analyzed by an online gas chromatography (Tianmei GC-7806).

References

1. Jaramillo, T. F. *et al.* Identification of Active Edge Sites for Electrochemical H_2 Evolution from MoS_2 Nanocatalysts. *Science* **317**, 100–102 (2007).
2. Das, S. *et al.* A Self-Limiting Electro-Ablation Technique for the Top-Down Synthesis of Large-Area Monolayer Flakes of 2D Materials. *Scientific Reports* **6**, 28195 (2016).
3. Liao, L. *et al.* MoS_2 Formed on Mesoporous Graphene as a Highly Active Catalyst for Hydrogen Evolution. *Adv. Funct. Mater.* **23**, 5326–5333 (2013).
4. Liu, X. *et al.* Fabrication of 3 D Mesoporous Black TiO_2/MoS_2/TiO_2 Nanosheets for Visible-Light-Driven Photocatalysis. *Chemsuschem* **9**, 1118 (2016).
5. Lukowski, M. A. *et al.* Enhanced Hydrogen Evolution Catalysis from Chemically Exfoliated Metallic MoS_2 Nanosheets. *J. Am. Chem. Soc.* **135**, 10274–10277 (2013).
6. Nam, H. *et al.* MoS_2 transistors fabricated via plasma-assisted nanoprinting of few-layer MoS_2 flakes into large-area arrays and Chhowalla, M. Conducting MoS_2 Nanosheets as Catalysts for Hydrogen Evolution Reaction. *ACS Nano* **7**, 5870 (2013).
7. Nie, Z. *et al.* Ultrafast carrier thermalization and cooling dynamics in few-layer MoS_2. *ACS Nano* **8**, 10931–40 (2014).
8. Yin, Z. *et al.* Single-Layer MoS_2 Phototransistors. *ACS Nano* **6**, 74–80 (2012).
9. Eda, G. *et al.* Photoluminescence from Chemically Exfoliated MoS_2. *Nano Lett.* **11**, 5111–5116 (2011).
10. Wang, Y. *et al.* MoS_2-Coated Vertical Graphene Nanosheet for High-Performance Rechargeable Lithium-Ion Batteries and Hydrogen Production. *NPG Asia Mater.* **8**, 268 (2016).
11. Ho, W., Yu, J. C., Lin, J., Yu, J. & Li, P. Preparation and Photocatalytic Behavior of MoS_2 and WS_2 Nanocluster Sensitized TiO_2. *Langmuir* **20**, 5865–5869 (2004).
12. Tongay, S. *et al.* Thermally Driven Crossover from Indirect toward Direct Bandgap in 2D Semiconductors: $MoSe_2$ versus MoS_2. *Nano Lett.* **12**, 5576–5580 (2012).
13. Han, S. W. *et al.* Band-gap transition induced by interlayer van der Waals interaction in MoS_2. *Phys. Rev. B* **84**, 045409 (2011).
14. Frame, F. A. & Osterloh, F. E. CdSe-MoS_2: A Quantum Size-Confined Photocatalyst for Hydrogen Evolution from Water under Visible Light. J. Phys. *Chem. Commun.* **114**, 10628–10633 (2010).
15. Xiang, Q., Yu, J. & Jaroniec, M. Synergetic Effect of MoS_2 and Graphene as Cocatalysts for Enhanced Photocatalytic H_2 Production Activity of TiO_2 Nanoparticles. *J. Am. Chem. Soc.* **134**, 6575–6578 (2012).
16. Shen, M. *et al.* MoS_2 Nanosheet/TiO_2 Nanowire Hybrid Nanostructures for Enhanced Visible-light Photocatalytic Activities. *Chem. Commun.* **50**, 15447–15449 (2014).
17. Bai, S., Wang, L., Chen, X., Du, J. & Xiong, Y. Chemically exfoliated metallic MoS_2 nanosheets: A Promising Supporting Co-catalyst for Enhancing the Photocatalytic Performance of TiO_2 nanocrystals. *Nano Res.* **8**, 175–183 (2015).
18. Zheng, X. *et al.* Space-Confined Growth of MoS_2 Nanosheets within Graphite: The Layered Hybrid of MoS_2 and Graphene as an Active Catalyst for Hydrogen Evolution Reaction. *Chem. Mater.* **26**, 2344–23539 (2014).
19. Chang, K. *et al.* MoS_2/Graphene Cocatalyst for Efficient Photocatalytic H_2 Evolution under Visible Light Irradiation. *ACS Nano* **7**, 7078–7087 (2014).
20. Drescher, T., Niefind, F., Bensch, W. & Grünert, W. Sulfide Catalysis without Coordinatively Unsaturated Sites: Hydrogenation, Cis—Trans Isomerization, and H_2/D_2 Scrambling over MoS_2 and WS_2. *J. Am. Chem. Soc.* **134**, 18896–18899 (2012).
21. Wi, S. *et al.* Enhancement of photovoltaic response in multilayer MoS_2 induced by plasma doping. *ACS Nano* **8**, 5270 (2014).
22. Li, Y., Wang, H. & Peng, S. Tunable Photodeposition of MoS_2 onto a Composite of Reduced Graphene Oxide and CdS for Synergic Photocatalytic Hydrogen Generation. *J. Phys. Chem. C.* **118**, 19842–19848 (2014).
23. Tan, F. *et al.* Rough gold films as broadband absorbers for plasmonic enhancement of TiO_2 photocurrent over 400–800 nm. *Scientific Reports* **6**, 33049 (2016).
24. Zhou, W. *et al.* Ordered Mesoporous Black TiO_2 as Highly Efficient Hydrogen Evolution Photocatalyst. *J. Am. Chem. Soc.* **136**, 9280–9283 (2014).
25. Pan, X., Yang, M.-Q., Fu, X., Zhang, N. & Xu, Y.-J. Defective TiO_2 with oxygen vacancies: synthesis, properties and photocatalytic applications. *Nanoscale* **5**, 3601–3614 (2013).
26. Choi, H., Sofranko, A. C. & Dionysiou, D. D. Nanocrystalline TiO_2 Photocatalytic Membranes with a Hierarchical Mesoporous Multilayer Structure: Synthesis, Characterization, and Multifunction. *Adv. Funct. Mater.* **16**, 1067–1074 (2006).
27. Gao, X. *et al.* Enhanced Visible Light Photocatalytic Performance of CdS Sensitized TiO_2 Nanorod Arrays Decorated with Au Nanoparticles as Electron Sinks. *Scientific Reports* **7**, 973 (2017).
28. Zhou, W. *et al.* Synthesis of Few-Layer MoS_2 Nanosheet-Coated TiO_2 Nanobelt Heterostructures for Enhanced Photocatalytic Activities. *Small* **1**, 140–147 (2013).
29. Dai, R. *et al.* Epitaxial Growth of Lattice-Mismatched Core–Shell TiO_2@MoS_2 for Enhanced Lithium-Ion Storage. *Small* **12**, 2792–2799 (2016).
30. Liu, X. *et al.* Fabrication of 3D Flower-Like Black N-TiO_2-x@MoS_2 for Unprecedented-High Visible-Light-Driven Photocatalytic Performance. *Appl. Catal. B: Environ.* **201**, 119–127 (2017).
31. Zheng, L., Han, S., Liu, H., Yu, P. & Fang, X. Hierarchical MoS_2 Nanosheet@TiO_2 Nanotube Array Composites with Enhanced Photocatalytic and Photocurrent Performances. *Small* **12**, 1527–1536 (2016).
32. Ma, B., Guan, P.-Y., Li, Q.-Y., Zhang, M. & Zang, S.-Q. MOF-Derived Flower-like MoS_2 @TiO_2 Nanohybrids with Enhanced Activity for Hydrogen Evolution. *ACS Appl. Mater. Interfaces* 8, (26794–26800 (2016).
33. Li, H. *et al.* Few-layered MoS_2 nanosheets wrapped ultrafine TiO_2 nanobelts with enhanced photocatalytic Property. *Nanoscale* **8**, 6101–6109 (2016).
34. Yuan, Y.-J. *et al.* Constructing r TiO_2 Nanosheets with Exposed (001) Facets/Layered MoS_2 Two-Dimensional Nanojunctions for Enhanced Solar Hydrogen Generation. *ACS Catal.* **6**, 532–541 (2016).
35. He, H. *et al.* MoS_2/TiO_2 Edge-On Heterostructure for Efficient Photocatalytic Hydrogen Evolution. *Adv. Energy Mater.* **6**, 1600464 (2016).

36. Bai, S., Wang, L., Chen, X., Du, J. & Xiong, Y. Chemically exfoliated metallic MoS_2 nanosheets: A promising supporting co-catalyst for enhancing the photocatalytic performance of TiO_2 nanocrystals. *Nano Res.* **8**, 175–183 (2015).
37. Mock, J. J. *et al.* Distance-Dependent Plasmon Resonant Coupling between a Gold Nanoparticle and Gold Film. *Nano Lett.* **8**, 2245–2252 (2008).
38. Yang, Y., Matsubara, S., Nogami, M., Shi, J. & Huang, W. One-Dimensional Self-Assembly of Gold Nanoparticles for Tunable Surface Plasmon Resonance Properties. *Nanotechnology* **17**, 2821–2827 (2006).
39. Zhu, X. *et al.* Enhanced Light−Matter Interactions in Graphene-Covered Gold Nanovoid Arrays. *Nano Lett.* **13**, 4690–4696 (2013).
40. Lee, J., Lee, S., Kim, M. S., Shin, H. & Kim, J. Enhancement of Light-Matter Interaction and Photocatalytic Efficiency of Au/TiO_2 Hybrid Nanowires. *Opt. Express* **24**, 15171 (2016).
41. Wang, J.-H. *et al.* Ceria-Coated Gold Nanorods for Plasmon-Enhanced Near-Infrared Photocatalytic and Photoelectrochemical Performances. *J. Phys. Chem. C* **120**, 14805–14812 (2016).
42. Ma, L. *et al.* Improved Hydrogen Production of Au–Pt–CdS Hetero-Nanostructures by Efficient Plasmon-Induced Multipathway Electron Transfer. *Adv. Funct. Mater.* **26**, 6076–6083 (2016).
43. Tsukamoto, D. *et al.* Gold Nanoparticles Located at the Interface of Anatase/Rutile TiO_2 Particles as Active Plasmonic Photocatalysts for Aerobic Oxidation. *J. Am. Chem. Soc.* **134**, 6309–6315 (2012).
44. Mukherjee, B. *et al.* Exciton Emission Intensity Modulation of Monolayer MoS_2 via Au Plasmon Coupling. *Scientific Reports* **7**, 41175 (2017).
45. Bhanu, U., Islam, M. R., Tetard, L. & Khondaker, S. I. Photoluminescence quenching in gold-MoS_2 hybrid nanoflakes. *Scientific Reports* **4**, 5575 (2014).
46. Xiao, F. Layer-by-Layer Self-Assembly Construction of Highly Ordered Metal-TiO_2 Nanotube Arrays Heterostructures (M/TNTs, M = Au, Ag, Pt) with Tunable Catalytic Activities. *J. Phys. Chem. C* **116**, 16487–16498 (2012).
47. Bian, Z., Tachikawa, T., Zhang, P., Fujitsuka, M. & Majima, T. Au/TiO_2 Superstructure-Based Plasmonic Photocatalysts Exhibiting Efficient Charge Separation and Unprecedented Activity. *J. Am. Chem. Soc.* **136**, 458–465 (2014).
48. Pu, Y.-C. *et al.* Au Nanostructure-Decorated TiO_2 Nanowires Exhibiting Photoactivity Across Entire UV-visible Region for Photoelectrochemical Water Splitting. *Nano Lett.* **13**, 3817–3823 (2013).
49. Shi, Y. *et al.* Hot Electron of Au Nanorods Activates the Electrocatalysis of Hydrogen Evolution on MoS_2 Nanosheets. *J. Am. Chem. Soc.* **137**, 7365–7370 (2015).
50. Liu, B. & Aydil, E. S. Growth of Oriented Single-Crystalline Rutile TiO_2 Nanorods on Transparent Conducting Substrates for Dye-Sensitized Solar Cells. *J. Am. Chem. Soc.* **131**, 3985–3990 (2009).
51. And, B. N. & El-Sayed, M. A. Preparation and Growth Mechanism of Gold Nanorods (NRs) Using Seed-Mediated Growth Method. *Chem. Mater.* **15**, 1957–1962 (2003).

Acknowledgements

We thank Yaoyao Ren, Jinwen Yang and Qiang Fu for the TEM and SEM measurement. This work was supported by the Natural Science Foundation of China (11374236 and 11674254) and China Postdoctoral Science Foundation (2016M602338 and 2017M612762).

Author Contributions

Y.Y.L., J.H.W. and Z.J.L. contributed equally to this work. Y.Y.L. prepared the samples and conducted the experiments. J.H.W. and Z.J.L. assisted in the experiment. K.C. assisted in the experiment about hydrogen evolution tests. L.M. and Z.Q.C. supported the TEM and SEM measurement. The manuscript was written through contributions of all authors. All authors have given approval to the final version of the manuscript. S.J.D. and L.Z. revised the main manuscript text. Q.Q.W. conceived the idea and supervised the experiments.

Additional Information

Supplementary information accompanies this paper at doi:10.1038/s41598-017-07601-1

Competing Interests: The authors declare that they have no competing interests.